Retraction for *RSC Advances*:

Laser-induced gold/chitosan nanocomposites with tailored wettability applied to multi-irradiated microfluidic channels

Fabrizio Spano, Alessandro Massaro, Laura Blasi, Roberto Cingolani and Athanassia Athanassiou

RSC Adv., 2012, DOI: 10.1039/C2RA21452K. **Retraction published 2nd October 2012**

We, the named authors, hereby wholly retract this *RSC Advances* article. This article was submitted for publication without the knowledge and approval of all the co-authors listed.

Signed: Fabrizio Spano, Alessandro Massaro, Laura Blasi, Roberto Cingolani and Athanassia Athanassiou, October 2012

Retraction endorsed by Sarah Ruthven, Managing Editor, *RSC Advances*

RSC Advances

Accepted Manuscript

This is an *Accepted Manuscript*, which has been through the RSC Publishing peer review process and has been accepted for publication.

Accepted Manuscripts are published online shortly after acceptance, which is prior to technical editing, formatting and proof reading. This free service from RSC Publishing allows authors to make their results available to the community, in citable form, before publication of the edited article. This *Accepted Manuscript* will be replaced by the edited and formatted *Advance Article* as soon as this is available.

To cite this manuscript please use its permanent Digital Object Identifier (DOI®), which is identical for all formats of publication.

More information about *Accepted Manuscripts* can be found in the **Information for Authors**.

Please note that technical editing may introduce minor changes to the text and/or graphics contained in the manuscript submitted by the author(s) which may alter content, and that the standard **Terms & Conditions** and the **ethical guidelines** that apply to the journal are still applicable. In no event shall the RSC be held responsible for any errors or omissions in these *Accepted Manuscript* manuscripts or any consequences arising from the use of any information contained in them.

RSC Publishing

www.rsc.org/advances
Registered Charity Number 207890

RSC Publishing RSC Advances

LASER-INDUCED GOLD/CHITOSAN NANOCOMPOSITES WITH TAILORED WETTABILITY APPLIED TO MULTI-IRRADIATED MICROFLUIDIC CHANNELS

Journal:	*RSC Advances*
Manuscript ID:	RA-ART-07-2012-021452.R1
Article Type:	Paper
Date Submitted by the Author:	07-Sep-2012
Complete List of Authors:	Spano, Fabrizio; Italian Inst. Tech., massaro, alessandro; IIT@CBN, cingolani, roberto; IIT Genova, athanassiou, athanassia; IIT@CBN,

LASER-INDUCED GOLD/CHITOSAN NANOCOMPOSITES WITH TAILORED WETTABILITY APPLIED TO MULTI-IRRADIATED MICROFLUIDIC CHANNELS

Fabrizio Spano,[1*] Alessandro Massaro,[1*] Laura Blasi,[2] Roberto Cingolani,[3] Athanassia Athanassiou [1,3]

[1]Center for Biomolecular Nanotechnologies @UNILE, Istituto Italiano di Tecnologia (IIT), via Barsanti, 73010 Arnesano, Lecce, Italy
[2]National Nanotechnology Laboratory (NNL), CNR-Istituto Nanoscienze, via per Arnesano 73100 Lecce, Italy
[3]Istituto Italiano di Tecnologia (IIT), via Morego 30, 16163 Genova, Italy

*fabrizio.spano@iit.it, alessandro.massaro@iit.it

ABSTRACT

The controlled wettability of gold nanocomposite surfaces obtained by laser irradiation is introduced. Starting from the conception of materials with controlled surface properties, we describe all the different steps to generate the gold functionalized nanocomposite material and illustrate its surface wettability. Photopatterned gold polymeric films are performed in order to exhibit a remarkable decrease in their wettability when UV laser light irradiation is applied. This process is totally controlled by means of laser texturing allowing the generation of localized areas with tunable wettability by controlling accurately the laser irradiation time. This new technique named laser texturing on gold nanocomposite materials (LTGNM) is applied on chitosan (CTO) polymer with a gold precursor ($HAuCl_4$) suitable for the proposed LTGNM approach. The introduction of a formation mechanism of gold particles is formulated and corroborated by preliminary experimental observations. The control of the irradiation times participates and proves the fragmentation process of the gold nanoparticles (Au-NPs). This new ability of gold nanocomposite material (GNM) provides new potential applications and a possible upscaling in microfluidics and in particular in lab on chip devices for liquid spreading or drugs transports. A microfluidic device based on the control of laser textured CTO-Au surface is proposed. In particular we propose an innovative microfluidic channel constituted by different spatial steps with modified contact angle regions for liquid spreading.

KEY WORDS: Gold Precursor, Nanoparticles, Chitosan, Nanocomposites, Laser Texturing, Photopatterning, Wettability, Microfluidic channel.

1. INTRODUCTION

Surface wettability control is attractive in various applications for a wide range of domains as industry, medicine and agriculture [1-6]. In particular, if the surfaces can be modified from hydrophobic to hydrophilic by a simple technique, the issue becomes suitable for microfluidics. Different techniques and applications where the control of the wettability is fundamental have been developed in microfluidics for chemical and biochemical analysis [7-13]. Controlling surface wettability may be the simplest approach for microfluid control. In a microchannel, the microfluid flow is strongly affected by the surface wettability due to the large specific interface. Indeed, water can be easily introduced into hydrophilic microchannels, while, in the case of hydrophobic channels, additional external pressure is required. Combining polymers and nanofillers properties, nanocomposite materials can be turned from hydrophobic into hydrophilic surface materials, preserving their flexibility and easy processability. Therefore, by controlling the size of the generated metallic particles, we may control the properties of the material providing new applications.

In this work an innovative approach of surface properties control by laser texturing process is introduced. By UV laser light irradiation, we are able to control the surface wettability of a chitosan (CTO) polymeric film in which is introduced a chloroauric acid salt ($HAuCl_4$) by immersion [14]. Specifically, the UV irradiation is responsible for the creation of gold nanoparticles (GNPs) in precise irradiated surfaces of the polymeric film. This new technique named laser texturing on gold nanocomposite materials (LTGNM) is applied on CTO polymer with gold precursor. The process is possible due to the ability of CTO polymer to behave as a hydrogel when use in high concentration [15-17]. This process also allows us to localize and design accurately surface patterns and moreover to tune metallic particle size in the range of nanoscale by playing with the laser irradiation time, fluencies and/or with the laser working wavelength. Simultaneously with the description of this innovative patterning technique, we will comment the gold particle formation under our experimental conditions. Reported works already describe metallic nanometer-sized particles formation by laser irradiation starting from laser ablation to more classical photoactivity [18].

In our work, we will focus on the hypothesis of a fragmentation mechanism occurring by laser irradiation. These hypotheses required the use of high-intensity laser excitation. Nevertheless, as described in literature, even simple shape modifications can occur at low intensity excitation. In particular, photofragmentation of silver nanoclusters is described by Kamat [19-21]: the laser pulse excitation is able to fragment silver particles with sizes ranging from 60nm to 5nm. In the opposite direction, photofusion of metal nanoclusters have been illustrated in literature. Observations of fused aggregates have been characterized forming large segregated spherical particles. In order to corroborate this result, several works [22-25] describe laser-induced melting or fragmentation of larger particles into smaller spherical particles. The formation of aggregates forming large size spherical particles is described after long duration laser irradiation (532nm - 30 minutes)

indicating the formation of fused particles. Moreover, by radiation chemical method, Henglein et al [26] reports about the enlargement of gold particles: the technique allows to enlarge gold particles to any desired size (until 120nm). At moderate energies (μJ), Link et al [27, 28] illustrates the photofragmentation of nanorods by laser irradiation using the 800nm wavelength: it is demonstrated even the influence of the laser pulses duration with the generation of nanorods-shaped particles with femtosecond laser pulses (100 fs) and the generation of very small near-spherical particles with nanosecond pulses (7 ns). At high energies (mJ), fragmentation is also observed for the femtosecond pulses irradiation. It is important to notice that the same per pulse energy leads to different results when the particles are exposed to femtosecond or nanosecond laser pulses.

As novelty, analyzing all the reported works, we have implemented all the size-controlling process correlated to wettability property into a solid polymeric film able to transport generic liquids. We will focus on these morphological changes caused by laser irradiation to build a first hypothesis of formation mechanism of gold particles occurring in CTO polymer film. Based on this mechanism we design and fabricate a lab on chip channel. We organize the work as follows:

- 1) we propose the design of a microfluidic channel based on the principle of contact angle variation.
- 2) we characterize the CTO-Au material in order to realize a preliminary study of the basic used material.
- 3) we apply a innovative laser texturing technique able to improve variation of contact angle surface by controlling GNPs patterning.
- 4) finally we prove the basic principle of droplet spreading by means of a single channel experimental results.

2. DESIGN AND BASIC PRINCIPLES OF CONTROLLED WETTABILITY CHANNELS

In Fig. 1 (a) is shown an example of lab on chip for read-out application. In the proposed layout 4 microfluidic channels are considered. Each channel is characterized by a gradient of GNPs density of the CTO-Au surface. The different spatial step of densities allows to spread a droplet along the channel until a chip (output of the device) able to read and process the information associated to the droplet. Simultaneously all the channels can be used for a real time response: each chip can be suitable for different kind of analysis as happens for blood analysis (DNA reading [29], diabetes analysis, etc…). The chip could be integrated on the same CTO device. Photonic crystals technology can be also used for the reading chip fabrication in order to perform a high efficiency optical bio-sensor [29]-[30]. The droplet to analyze is deposited on the central region of the device. Based on this principle we design

and fabricate a single channel of the lab on chip device by providing new technological implementation for microfluidic applications.

3. CHEMICAL CTO-Au CHARACTERIZATION

Chitosan, as illustrated in Figure 2, is a natural biodegradable and biocompatible polysaccharide polymer derived from chitin (the second most naturally abundant polysaccharide on the planet to cellulose), a linear chain of acetylglucosamine groups, extracted from crustacean shells and the cell walls of many fungi. For these reasons, the CTO polymer is ideal for biological applications. CTO polymer is known to form hydrogels. As CTO is soluble in weak acids due to the low p*K*a of approximately 6.5, and once in solution, protonation of the amino groups gives CTO a cationic nature [31]. For the preparation of the polymeric films, CTO polymer (Sigma Aldrich - 448877) was initially dissolved in acetic acid (1% - Sigma Aldrich - 242853). Various concentrations of CTO polymer solutions (0.5%, 1% and 2% in weight) are prepared. CTO polymeric films were obtained by drop-casting (50µL/cm^2). The use of the specific CTO concentrations allows the formation of CTO hydrogels [32] able to absorb the Au precursor. The precursor used is a chloroauric acid salt (Sigma Aldrich – 254169, Mw($HAuCl_4$) = 339.5 g/mol) and was dissolved in distilled water ([Au]=0.01M; [Au]=0.02M). The precursor was introduced in the CTO polymeric film by immersion of the latter in the water solution of the former. Immersion times allow tuning of the precursor concentration introduced into the CTO polymeric films, reaching saturation after 60 minutes of immersion time. The generation of Au NPs is avoided during the immersion phase. The thickness of the CTO films obtained by drop-casting is between 2 and 5 µm and is function of the CTO solution concentration [32]. Octadecylamine (Sigma Aldrich – 74750, Mw($C_{18}H_{39}N$) = 269.51 g/mol) is used for functionalization of the gold patterns after laser texturing allowing to control their contact angle. Octadecylamine is mixed with ethanol ([C]=15mM). CTO-Au samples are immersed for 40 minutes in the octadecylamine solution for functionalization. For the initiation of the formation of the Au NPs the precursor photolysis is essential.

The hydrogel nature of the CTO film results in the tendency to absorb ambient moisture or liquids if in solution. CTO hydrogels have been shown to swell in response to the changes in pH and humidity [33]. This hydrogel nature can result in swelling problems and reduces chemical robustness. In this work, gold precursors were introduced in the CTO polymer thin films. By controlling the immersion time of the polymer film in the precursor solution, different composite hydrogel structures were obtained with varying precursor concentrations [34, 35]. In Figure 3 (a), are illustrated FT-IR spectra of CTO films with increasing precursor concentrations ([Au=0.01M]) due to increasing immersion times (starting from 20 minutes to 60 minutes) in the precursor solutions. In particular the FT-IR measurements illustrated in Figure 3(a), were made on a 0.5% CTO polymer film. The comparison between the 20 minutes immersion curve (black) with the two 40 minutes (red)

and 60 minutes (blue) immersion curves clearly demonstrates the increased precursor concentration in the case of longer immersion times by the increase in their absorption intensity. The superposition of the 40 and 60 minutes immersion curves indicates the saturation of the film. As illustrated in the FTIR spectra in Figure 3 (b), changing the CTO polymer concentration and keeping constant the immersion time, an increase of the absorption intensity occurs for 1% CTO film with respect to the 0.5% CTO film, indicating that the former absorbs more Au precursor than the latter. We have observed that increasing the CTO concentration an increase of the film thickness occurs [32]. Saturation of the Au precursor concentration is reached for immersion time about 60 min for a CTO concentration of 1% (about 3 µm of thickness). CTO polymer is known to be a good stabilizing/reducing agent of Au precursors [36]. Nevertheless, in our case, as the precursor is introduced after the formation of the drop-casted CTO film and not in solution, the reduction process needs to be stimulated by an external excitation. The solution is presented in the next section.

4. LASER TEXTURING ON GOLD NANOCOMPOSITE MATERIALS (LTGNM)

The photolysis is realized by UV laser light. The laser used is a Nd:YAG laser (Quanta-Ray GCR-190, Spectra Physics) operating at 10 Hz with 4-6 ns pulse duration as illustrated in experimental setup of Fig. 4. The wavelength used for all our experiments is 355 nm. The laser irradiation is realized at room temperature with a relative humidity of 30-60%. Absorption spectra of the CTO-Au GNPs films were done with a UV-Visible spectrophotometer (VARIAN Cary 300 Scan). Fourier transform infrared spectroscopy (FT-IR) spectra were realized with a VERTEX 70 FT-IR instrument in the spectral range defined from 4000 to 1500 cm^{-1} in absorbance mode. For AFM images, a Park System AFM instrument (XE-100) was used in true non-contact mode. The images were realized in air using an anti-vibration table (Table Stable TS-150) and an acoustic enclosure. Single-beam silicon cantilevers tips (PPP-NCHR-10) were used for the data acquisition with about less than 10 nm nominal radius and 42 N/m elastic force constant for high sensitivity. The resonance frequency was defined around 280 kHz. The scan rate was between 0.2 and 1.0 Hz. Optical microscopy images were realized with a Zeiss AXIO instrument. Scanning electron microscopy (SEM) images were taken using a FEI NOVA nanoSEM 200 scanning electron microscope. The measurements are realized in low vacuum with a pressure of 0.6mbar and by using a Helix detector at a tension of 17.5 kV. By generating GNs on the top of hydrogel material, it will be possible to control the spreading of droplets on the surface.

We use for our specific applications an UV light generated be a laser source at 355 nm wavelength. The use of UV laser light allows us to generate photolytic GNPs at the surface of the CTO-Au polymer film. Moreover, the generation is localized at precise areas where laser texturing will be addressed. Specific patterning can be generated. The size of the patterned gold surfaces is directly dependent on the size of the laser beam which is function of the

optical system used during the experimentation. The smallest gold surface generated has a resolution of several hundreds of microns. The CTO-Au films are irradiated with UV laser light in wet air at controlled room temperature (20°C). Immediately after the laser irradiation, the film maintained the original color from few minutes to hours depending on the irradiation time until it starts to change color in the localized irradiated area from a pale blue-violet until clear gold mirror layout. We define the time needed to obtain the complete photolytic reaction as "a relaxation time" indicating the long duration of the process to obtain a stable gold/CTO film. The variation of color, in particular, all the panel of colors from pale blue to dark violet indicates the formation of colloidal gold. The color is directly linked to the irradiation time and to the size of the colloidal gold particles. A prolonged irradiation provides a metallic luster (after 3 min with high laser intensity) but observed only after a prolonged "relaxation time" into a clear gold mirror. This variation of color can be correlated to the variation of absorption spectra. The full characterization of the formed GNPs and the "relaxation time" effect will be addressed elsewhere. The defined "relaxation time" used during our experiments is fixed to 24 hours.

After irradiation, the colloidal absorption band of gold appeared around 550-580 nm. As described by Duff et al [37, 38], the $AuCl_4$ ions decrease in favor of the colloidal gold particles. The formation of photolytic gold causes the increase of absorbance at precise wavelength regions and the colloidal absorption band got broader [39] and forming finally bulk gold film [40, 41]. Figure 5(a) shows UV-Vis spectra obtained on a CTO-Au precursor film after different irradiation times. Figure 5(b) is a simplified plot of Fig. 5(a) illustrating only same significant irradiation times. The intensity of the spectra indicates that the quantity of gold particles generated linearly depends on the irradiation time as demonstrated in the inset of Figure 5(b). We observe that the absorption peak corresponding to the presence of GNPs increases in function of the irradiation time to reach a maximum after 60s irradiation time for the laser parameters used in the specific experiment. On the top, a shift of the maximum peak is observed in function of the irradiation time, which may be explained by the generation of different particle sizes. The trend is not clear due to the inhomogeneity of the generated particle sizes, which is further verified by the broadening of the spectra.

The generation of GNPs at the surface of the nanocomposite films in function of the irradiation time can be illustrated by Atomic Force Microscopy (AFM) images (Figure 6). Fig. 6(a) illustrates a non-irradiated area indicating a very smooth surface with a roughness of few nanometers. In absence of laser irradiation, no particles are observed on the top of the CTO polymeric films. Fig. 6(b) and (c) represent areas after 40 and 60 seconds laser irradiation time. At this stage, generation of GNPs are observed (particles with a size around 500 nm). By increasing even more the irradiation time to 80 s (Fig. 6(d)), the gold particle density seems to increase with a parallel reduction of their size (around 100 nm). In that laser intensity condition, the time necessary to obtain the maximum density of gold particles is around 80 seconds. In these experimental conditions, the density of gold particles becomes almost homogeneous and they form a sort of quasi continuous film on the top of

the surface film. Even the shape of the gold particles seems to change adopting spherical shapes after prolonged irradiation, whereas upon smaller irradiation times they seem more irregular. By increasing the irradiation time to a highly irradiated area (2 minutes) viewed by AFM technique (Fig. 6(e)), it seems that the gold/CTO film starts to melt and form an agglomeration of gold crystals and CTO polymer where the gold particles become difficult to discriminate. The analysis of the AFM phase images from Fig. 6 (a) to (d) indicates a phase variation at the precise position of the gold particles possibly explaining the fact that gold particles are directly exposed to air and not recovered by a polymeric layer.

In order to prove the AFM observations, we perform scanning electron microscopy (SEM) images analysis of the same irradiated samples. The CTO-Au films used for the SEM analysis are realized in the same experimental conditions. The only key parameter is the laser irradiation time. Figures 7(a) and (b) illustrate respectively the SEM image and the chemical analysis of the different elements of a nanocomposite area after 20 seconds of irradiation, indicating the presence of GNPs on the CTO polymeric film. In Figs 7 (c) and (d), SEM and chemical analysis images after a higher irradiation time (70 seconds) of a gold nanocomposite area, are shown respectively. The comparison of these two irradiation times confirms the AFM observations indicating the variation in size and density of the gold particles generated by laser irradiation, with particle size decreasing from around micrometer-sized particles to nanometer-sized particles (from 100 nm to 300nm) and increasing density. The photolysis of gold particles at the surface of the CTO films is apparently happening.

About the mechanism of formation, the analysis of the previous results confirms the creation of gold colloidal particles and the formation of gold clusters with different sizes. Growth of particles occurs normally by agglomeration and cluster formation [37-41]. These described mechanisms concern principally the laser ablation process and involve high laser intensities. Concerning the range of laser intensities used in our experiment, we can consider them sufficiently high to observe this category of growth mechanisms. Nevertheless, agglomeration mechanism cannot be confirmed in our experimental conditions. After in prolonged laser irradiation, the size of the particles is decreasing and becoming smaller and smaller reaching size closed to 100-200 nm. This decrease of size may be correlated to a specific fragmentation mechanism occurring in high laser intensities. For example, several works [42-49] indicate the formation of metal nanoparticles by laser ablation in water solution using various wavelengths. The variation of wavelength leads to a variation of size particles. The average diameter of the particles reduces with the wavelength by using very high laser intensities (around 40J/cm^2). The major mechanism used to describe this reducing size behavior is the fragmentation mechanism of colloidal particles by self-absorption of laser pulses. Other works indicate clearly the influence of chemically active species present in the solution and the laser parameters. In our case, the presence of the CTO polymer must be taken in consideration, particularly for its role of reducing/stabilizing agent by means of its concentration or the ratio between GPs concentration and CTO concentration.

Theoretical works indicate the possibility to melt small gold particles under strong thermal annealing processes [50]. Correlated with the hypothesis of laser-induced shape modifications by laser irradiation, these mechanisms indicate an interpretation of the size reduction mechanism observed in our experiments.

4.1. PHOTOFRAGMENTATION PROCESS

To demonstrate the hypothesis of GPs fragmentation process, we focus our attention on the analysis of AFM and SEM images by using defined conditions (fluence around 3 J/cm^2 and irradiation times at 70 seconds). In Figure 8 gold particles viewed by AFM images are represented. By focusing precisely on specific particles, it appears clearly that several particles seem to fragment. We can even observe particles already fragmented and starting to separate indicating a mobility mechanism maybe correlated with the size of the particles. This mobility may allow the gold particles to reach the surface of the CTO polymer film as observed previously via AFM phase images. The fragmentation mechanism as previously described is linked with absorption of laser pulses and by this way with an increase of local temperature due to the gold particles which may increase the mobility of the gold particles in the CTO polymeric film.

To illustrate the fragmentation principle, we schematize in Figure 8 (a) the fragmentation process occurring in the CTO-Au film as observed by SEM images in Figure 9 (b) where is also illustrated that the process is observed in the bulk at different depths (see cross-section of the inset of Fig. 9 (a). After the fragmentation process and by applying a prolonged irradiation time, it is possible to generate a quasi continuous gold patterns as schematically idealized in Fig. 9 (c) and proved by AFM images of Fig. 9 (d). An attentive observation of the images in Figure 9 indicates clearly the fragmentation of gold particles leading to the formation of smaller GNPs. This fragmentation mechanism leads to the formation of spherical gold nanoparticles starting from geometrical gold particles present in the CTO films.

AFM and SEM images allow us to observe this rare mechanism in a non-liquid system and to obtain images at different steps during the photofragmentation. Indeed, SEM and AFM images confirm the fragmentation mechanism of bigger particles in smaller ones. The laser fragmentation mechanism is often described in liquids, and linked with laser ablation process [41-49]. In our case, for the gold/CTO nanocomposite material, we can admit and transpose the interaction of the “laser-induced size reduction” observed in literature describing the gold particle fragmentation in small particles under laser fragmentation. These observations leads us to assume as principal mechanism of fragmentation the “laser-induced size reduction” and allows us, in a controlled manner, to tune the average size of the GNPs by selecting properly the laser intensities and the irradiation times. The fluence is defined around 3 J/cm^2 (this fluence value allows to not destroy the surface at low

irradiation time and allows to tune laser irradiation process) and the irradiation times from 50 to 80 seconds.

To confirm this nanoparticle size tuning, we will demonstrate how the wettability property of our gold/CTO nanocomposite materials can be controlled and useful for device applications as microchannel surfaces or other microfluidic control for lab on chips able to spread a droplet in a well defined direction. By generating GNPs on the top of the nanocomposite material, we expect to observe surface property modifications. As illustrated previously, the size and the density of the GNPs are modified by irradiation times at a fixed fluence. More the surface is irradiated, more the density of the GNPs increase and more their size decrease reaching nanometer scale. Their size and density seem time and fluence dependent and seem to influence the surface wettability. By measuring for each irradiation time as illustrated on Figure 10 the water contact angle, we observe that the irradiation time influences the wettability property of our gold nanocomposite material. It seems that the laser texturing of the CTO polymeric film allows modifications of the water contact angles. The information of the plot of the inset of Figure 10 is also reported in the insets of the same figure reporting the photo of the droplet with contact angles and the CTO surface viewed by AFM topography images. We observe clearly the decrease of water contact angle in function of the increasing irradiation time. As result, we can reach a very small contact angle value closed to 13°. By representing in Figure 11 cosines of the water contact angle versus the area fraction of gold nanoparticles, we observe a linear trend which can be correlated to the Cassie's equation. As expected the growth of gold nanoparticles on the top of the CTO polymer surface modify the surface roughness and by the way change the surface wettability following the Cassie's Law.

5. EXPERIMENTAL RESULTS: SINGLE MICROFLUIDIC CHANNEL

By using prolonged irradiation times, we observe on Figure 12 that the decrease of the water contact angle is followed by an important increase reaching almost 90° after 180 s irradiation time. The working range of the controlled wettability property is ranged from 10s to 180s and function of the laser fluence (Fluence ~ 3 J/cm^2). In Inset of Figure 12 (a), the obtained gold/CTO surface is illustrated by AFM topography images indicating a possible mixing between the CTO polymer and the gold nanoparticles. As illustrated in Fig. 12 b), after 180 seconds of irradiation time, it is possible to observe a degradation of the CTO polymer. These results indicate that we are able to control or tune the surface wettability of our gold/CTO nanocomposites by tailoring the irradiation times in a working range of Fig. 12 (a). We observe that this working range changes with the used fluence. We can generate from hydrophobic to hydrophilic surfaces just by using laser texturing at a precise irradiation time. Focusing on a possible channel droplet design, before functionalization of the CTO-Au

surface with octadecylamine, we irradiate adjacent regions on the same sample using different laser irradiation times as illustrated in Fig. 9 (a).

In order to explain the basic principle of the droplet spreading we consider the 3D finite element method (FEM) simulation of Fig. 13 representing the basic principle of the droplet spreading and separation. A water droplet is deposited between two regions of a CTO surface obtained by laser texturing: the region 1 of Fig. 13 (a) models the region with a lower density of GNPs (higher contact angle), besides the region 2 represents the region with higher density of GNPs (lower contact angle). According with the experimental results illustrated in the next section, we fix for boundary 1 of Figure 13 a contact angle of 50° and for boundary 2 a contact angle of 13°. The simulation help to understand the basic principle of the spreading and separation processes: in this figure it is clear that the droplet will be splitted in two parts allowing a directional spreading as happens for two opposite channels of Figure 1(a). Contact angle measurements were done using a KSV CAM 200 instrument. The sessile drop method was employed using distilled water with a typical drop volume around 10 µL. The objective is to generate a drop movement on large area (6mm) overcoming the wettability hysteresis phenomena by functionalizing the laser irradiated areas. But, at this point, we can only speak about droplet spreading as illustrated by our results. By creating three different gold patterned areas, the liquid spreading is rendered possible as illustrated in Fig. 14. The different laser conditions will allow us to create regions with controlled wettability. The droplet will be able to travel from one region to the other undisturbed by the hysteresis phenomena. These proposed three spatial steps represent the basic layout of the single channel reported in Fig. 1. Longer spatial steps with tuned laser intensities and the implementation of a 4-channel device with real drop movement are under investigation.

6. CONCLUSIONS

In this work we investigate the wettability control of a designed patterned gold nanocomposite material by laser texturing. We illustrate the transition from a hydrophobic surface to a hydrophilic one by generating a gold nanostructured polymeric surface. By tuning the surface properties using a controlled laser texturing technique which allows the generation of gold nanoparticles on the top of the CTO surface, we demonstrate the versatility of our unique material. This switch property can be implemented for devices which involve the drop spreading in a well-defined microchannel direction. The described process allows us to control the hydrophobicity of the CTO-Au polymeric film surface. After the characterization of our gold textured surfaces by atomic force and scanning electron microscopies, and by describing a first hypothesis about the GNs formation, we establish a correlation between surface wettability properties and GNs density controlled by the laser irradiation times for a defined fluence. The tuning process of the gold nanopatterning allows to control the spreading of different liquids having various viscosities as required in lab-on-

chip fluidics. We have succinctly highlighted the fragmentation mechanism of GNs in CTO polymer films which will be described in further works. Due to fragmentation mechanism, the variation of gold density on the CTO-Au surfaces can be directly used to modify their surface properties. Finally we propose a designed channel device based on the innovative laser texturing process on gold nanocomposite materials controlling wettability property on localized regions of the CTO-Au film in a multi-irradiated channel layout. Being the used material biocompatible, the microfluidic channels could be integrated in bio lab-on-chip able to screen simultaneously several read-out characterizations. The proposed LTGNM method could be substituted to the traditional lithography processes in order to improve gold uniform layouts suitable for lab-on-a-chip devices or nano bio sensors.

ACKNOLEDGEMENT

The authors gratefully thank the scientists Mario Malerba and Luigi Martiradonna.

REFERENCES

1. R. N. Wenzel, Resistance of solid surface to wetting by water, Ind. Eng. Chem. 1936, 28, 988-994.
2. A. B. D. Cassie, S. Baxter, Wettability of porous surfaces, Trans. Faraday Soc. 1944, 40, 546-561.
3. T. Onda, S. Shibuichi, N. Satoh, K. Tsujii, Super-water-repellent fractal surfaces, Langmuir 1996, 12, 2125-2127.
4. H. Y. Erbil, A. L. Demirel, Y. Avci, O. Mert, Transformation of a simple plastic into a superhydrophobic surface, Science 2003, 299, 1377-1380.
5. M. K. Chaudhury, G. M. Whitesides, How to make water run uphill, Science 1992, 256, 1539.
6. D. L. Schmidt, R. F. Jr. Brady, K. Lam, D. C. Schmidt, M. K. Chaudhury, Contact angle hysteresis, adhesion, and marine biofouling, Langmuir 2004, 20, 2830-2836.
7. B. He, N. A. Patankar, J. Lee, Multiple equilibrium droplet shapes and design criterion for rough hydrophobic surfaces, Langmuir 2003, 19, 4999-5003.
8. C. W. Extrand, Model for contact angles and hysteresis on rough and ultraphobic surfaces, Langmuir 2002, 18, 7991-7999.
9. S. A. Kulinich, M. Farzaneh, Effect of Contact Angle Hysteresis on Water Droplet Evaporation from Super-Hydrophobic Surfaces, Appl. Surf. Sci. 2009, 255, 4056–4060.
10. T. N. Krupenkin, J. A. Taylor, T. M. Schneider, S. Yang, From Rolling Ball to Complete Wetting: The Dynamic Tuning of Liquids on Nanostructured Surfaces, Langmuir 2004, 20, 3824–3827.
11. G. Londe, A. Chunder, L. Zhai, H. J. Cho, An Analytical Model for the Wettability Switching Characteristic of a Nanostructured Thermoresponsive Surface, Appl. Phys. Lett. 2009, 94, 164104/1–164104/3.
12. A. Zeira, D. Chowdhury, R. Maoz, J. Sagiv, Contact Electrochemical Replication of Hydrophilic Hydrophobic Monolayer Patterns, ACS Nano, 2008, 2, 2554–2568.
13. J. Yuan, X. Liu, O. Akbulut, J. Hu, S. L. Suib, J. Kong, F. Stellacci, Superwetting Nanowire Membranes for Selective Absorption, Nat. Biotechnol. 2008, 3, 332–336.
14. T. Miyama, Y. Yonezawa, Langmuir 20, 5918, (2004).
15. F.M. Goycoolea, W.M. Argüelles-Monal, J. Lizardi, C. Peniche, A. Heras, G. Galed, E.I. Díaz, Polymer Bulletin 58, 225–234 (2007).
16. H.T. Ta, C.R. Dass, D.E. Dunstan, J. Control Release, 20, 205 (2008).
17. M. Ishihara, K. Obara, S. Nakamura, M. Fujita, K. Masuoka, Y. Kanatani, B. Takase, H. Hattori, Y. Morimoto, M. Ishihara, T. Maehara, M. Kikuchi, J Artif., Organs, 9, 8–16 (2006).
18. P. V. Kamat, Phys. Chem. B 106, 7729 (2002).
19. P. V. Kamat, M. Flumiani, G. Hartland, *J. Phys. Chem. B* 1998, *102*, 3123.
20. A. Dawson, P. V. Kamat, P. V. *J. Phys. Chem. B* 2001, *105*, 960.
21. H. Fujiwara, S. Yanagida, P. V. Kamat, P. V. *J. Phys. Chem. B* 1999, *103*, 2589.
22. A. Takami, H. Yamada, K. Nakano, S. Koda, *Jpn. J. Appl. Phys.*1996, *35*, L781.
23. Y. Niidome, A. Hori, T. Sato, S. Yamada, *Chem. Lett.* 2000, 310.
24. R. C. Jin, Y. W. Cao, C. A. Mirkin, K. L. Kelly, G. C. Schatz, J. G. Zheng, *Science* 2001, *294*, 1901.
25. K. Murakoshi, H. Tanaka, Y. Sawai, Y. Nakato, *J. Phys. Chem.B* 2002, *106*, 3041.
26. A. Henglein, D. Meisel, Radiolytic control of the size of colloidal gold nanoparticles, Langmuir, 1998, 14, 7392-7396.
27. S. Link, C. Burda, M. B. Mohamed, B. Nikoobakht, M. A. El-Sayed, *J. Phys. Chem. A* 1999, *103*, 1165.
28. S. Link, Z. L. Wang, M. A. El-Sayed, *J. Phys. Chem. B* 2000,*104*, 6767.
29. K. Aoki**,** M. De Vittorio, T. Stomeo, F. Pisanello, A. Massaro**,** L. Martiradonna, S. Sabella, R. Rinaldi, Y. Arakawa, R. Cingolani, and P. Pompa , A method of identifying a target analyte using photonic crystal resonators, and related device Code: EP 09166989.5.
30. A. Massaro, "Theory, Modeling, Technology and applications of Micro/Nano quantum electronic and photonic devices," Transworld Research Network, IBN: 978-81-7895-498-1, 2011.
31. A. Domard and M. Domard, 2nd ed. New York: Marcel Dekker, 2002.

32. F. Spano, A. Massaro, R. Cingolani, A. Athanassiou, Optical enhancement by means of concentration tuning of gold precursors in polymer nanocomposite materials, Microelectronic Engineering, 88, 2011, 2763-2766.
33. J. Nunthanid, S. Puttipipatkhachorn, K. Yamamoto, and G. E. Peck, Drug Dev. Ind. Pharm., vol. 27, no. 2, pp. 143–157, 2001.
34. M. N. V. R. Kumar, React. Funct. Polym., vol. 46, no. 1, pp. 1–27, Nov. 2000.
35. Jim C. Cheng and Albert P. Pisano, J. MEMS, VOL. 17, NO. 2, 2008.
36. H. Huang, Q. Yuan, X. Yang, Journal of Colloid and Interface Science 282 2005, 26-31.
37. D. G. Duff, A. Baiker, P. P. Edwards, *Langmuir* 1993, *9*, 2301.
38. D. G. Duff, A. Baiker, I. Gameson, P. P. Edwards, *Langmuir* 1993, *9*, 2310.
39. A. Henglein, *Langmuir* 1999, *15*, 6738.
40. U. Kreibig, *J. Phys. (Paris)* 1977, *38*, C2-97.
41. R. E. Benfield, J. A. Creighton, D. G. Eadon, G. Schmid, *Z. Phys. D.* 1989, *12*, 533.
42. F. Mafune´, J. Kohno, Y. Takeda, and T. Kondow, H. Sawabe, *J. Phys. Chem. B* 2001, *105,* 5114-5120.
43. F. Mafuné, J. Kohno, Y. Takeda, and T. Kondow, *J. Phys. Chem. B*, 2000, 104 (35), pp 8333–8337.
44. F. Mafune´, J. Kohno, Y. Takeda, and T. Kondow, H. Sawabe, *J. Phys. Chem. B* 2000, *104,* 9111-9117.
45. S. Shukla and S. Seal, NanoStructured Materials, Vol. 11, No. 8, pp. 1181–1193, 1999.
46. F. A. Videla, G. A. Torchia, D. C. Schinca, L. B. Scaffardi, P. Moreno, C. Méndez, L. J. Giovanetti, J. M. Ramallo Lopez and L. Roso. JOURNAL OF APPLIED PHYSICS 107, 114308 2010.
47. E. Kadossov, U. Burghaus, Catal Lett (2010) 134:228–232.
48. A. V. Kabashin and M. Meunier, J. Appl. Phys. 94, 7941 (2003).
49. S. Barcikowski, A. Hahn, A.V. Kabashin, B.N. Chichkov, Appl. Phys. A 87, 47–55 (2007).
50. F. Ercolessi, W. Andreoni, E. Tosatti, Physical review letters, volume 66, number 7, 911-914.

LIST OF FIGURES

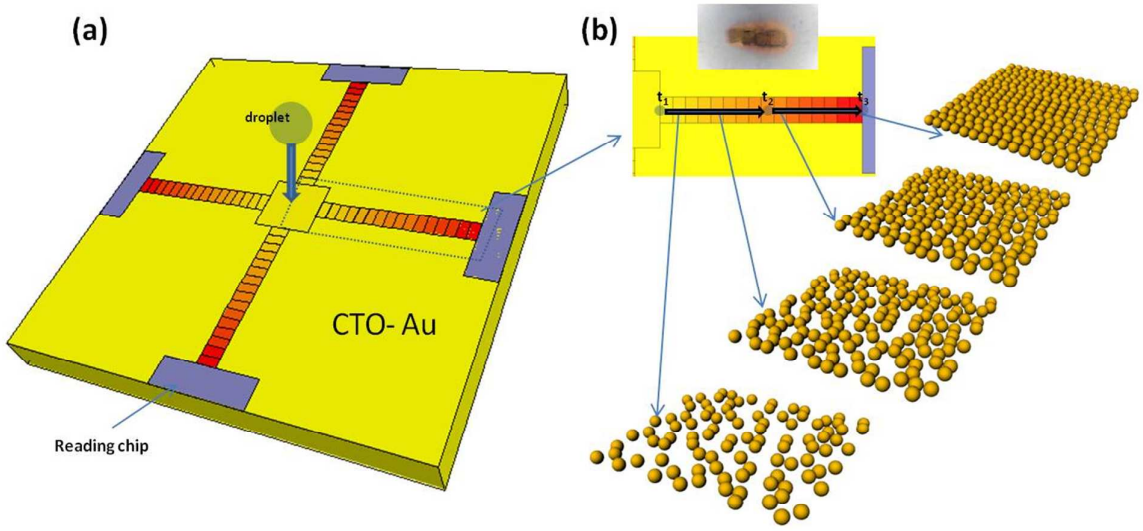

Figure 1: (a) 3D CTO –Au lab on chip CAD design device. (b) Zoomed single channel implementing different GNPs densities with an optical microscope image illustrating a small single channel.

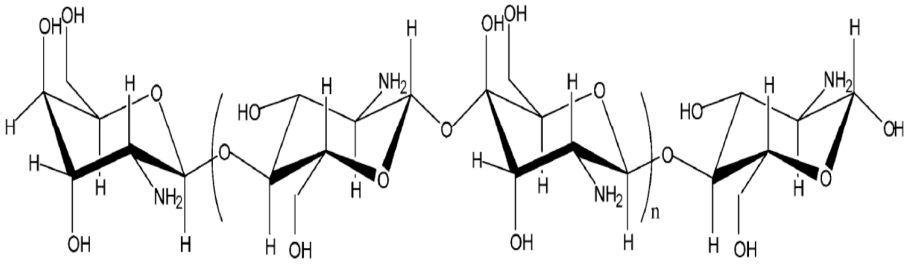

Figure 2: chemical structure of chitosan polymer.

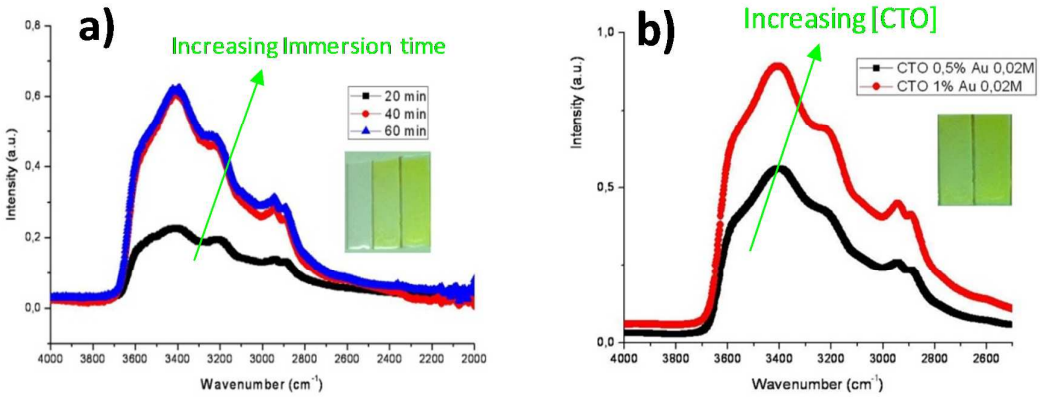

Figure 3: Hydrogel behavior of the CTO polymer illustrated by its ability to absorb Au precursors to form highly concentrated composite polymer films viewed by FT-IR. a) Influence of the immersion time on a 0.5% CTO film by using a precursor solution concentration of [Au]=0.01M; b) Influence of the CTO polymer concentration on the absorption intensity (precursor solution concentration: [Au]=0.02M, immersion time: 60 minutes).

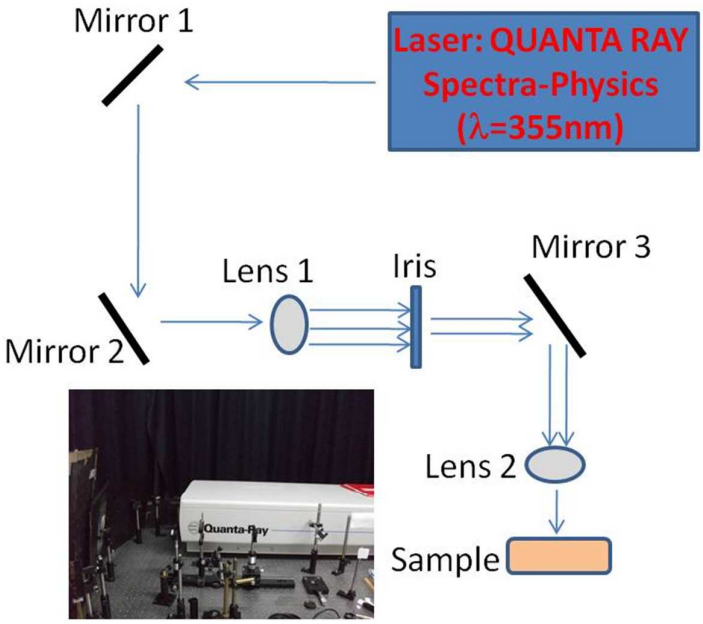

Figure 4: Experimental setup used to generate gold nanopatterned channels by LTGNM.

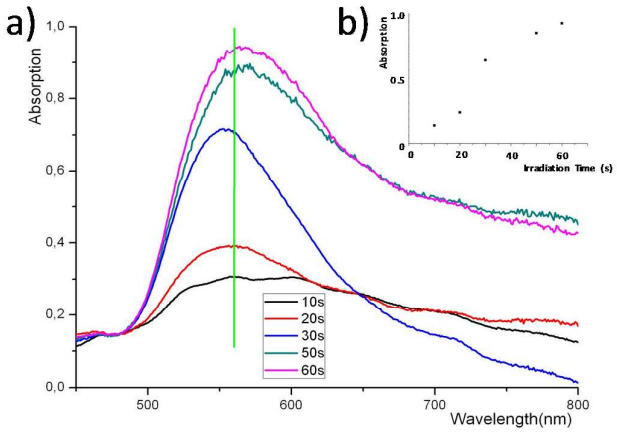

Figure 5: a) UV-Visible spectra illustrating the influence of the irradiation time from 10s to 60s time on 0.5 % CTO polymer films (Fluence 3J/cm^2). b) Inset: Illustration of the absorption behavior of the CTO-Au material in function of the irradiation time.

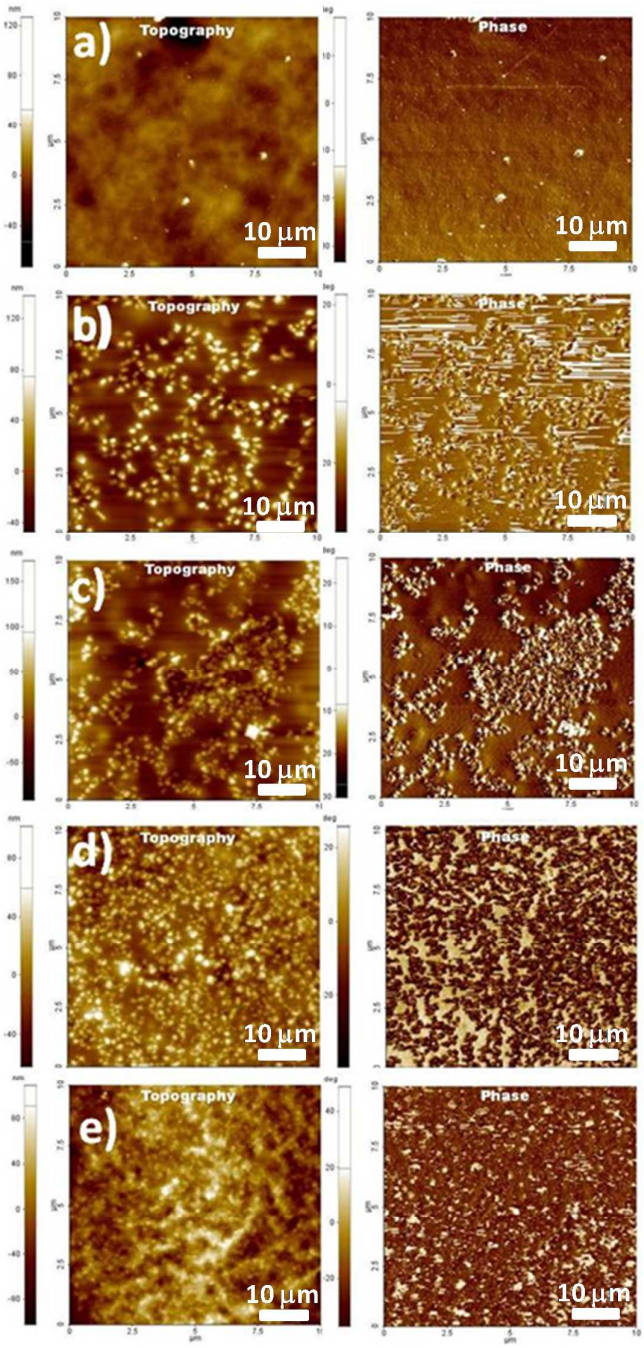

Figure 6: Evolution of the gold particle density and size in function of the irradiation time viewed by AFM images. Topography, error and phase AFM images for an area a) without irradiation, b) after 40 s laser irradiation, c) after 60 s laser irradiation and finally, d) after 80 s laser irradiation and e) after a prolonged laser irradiation (240s).

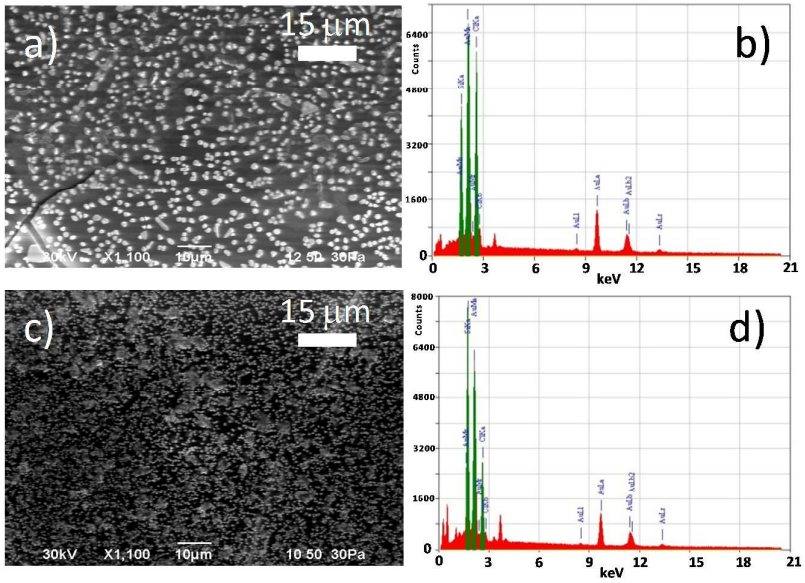

Figure 7: a) SEM image of the CTO polymer surface after 20 seconds irradiation time illustrating the presence of gold particles; b) Chemical analysis of the 20 seconds irradiated area indicating the presence of gold; c) SEM image of the CTO polymer surface after 70 seconds irradiation time illustrating the presence of gold particles; d) Chemical analysis of the 70 seconds irradiated area indicating the presence of gold.

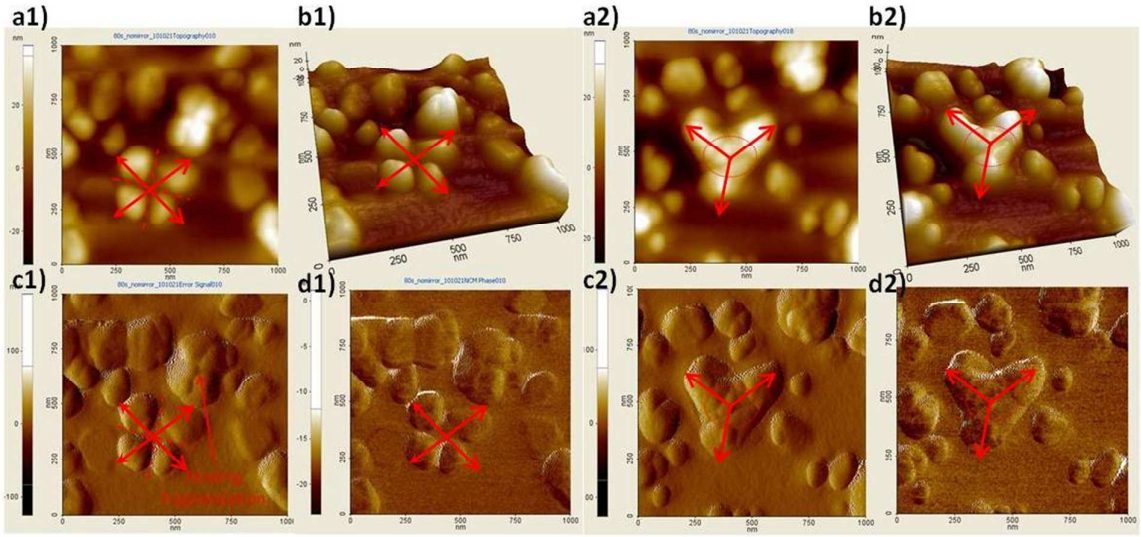

Figure 8: Illustration of the fragmentation mechanism hypothesis by laser irradiation viewed by AFM (laser irradiation intensity: 3 J/cm^2, irradiation time: 80s). Image 1: a1) 2D topography, b1) 3D topography, c1) error signal and d1) phase images of GPs fragmentation process. Image 2: a2) 2D topography, b2) 3D topography, c2) error signal and d2) phase images of GPs fragmentation process.

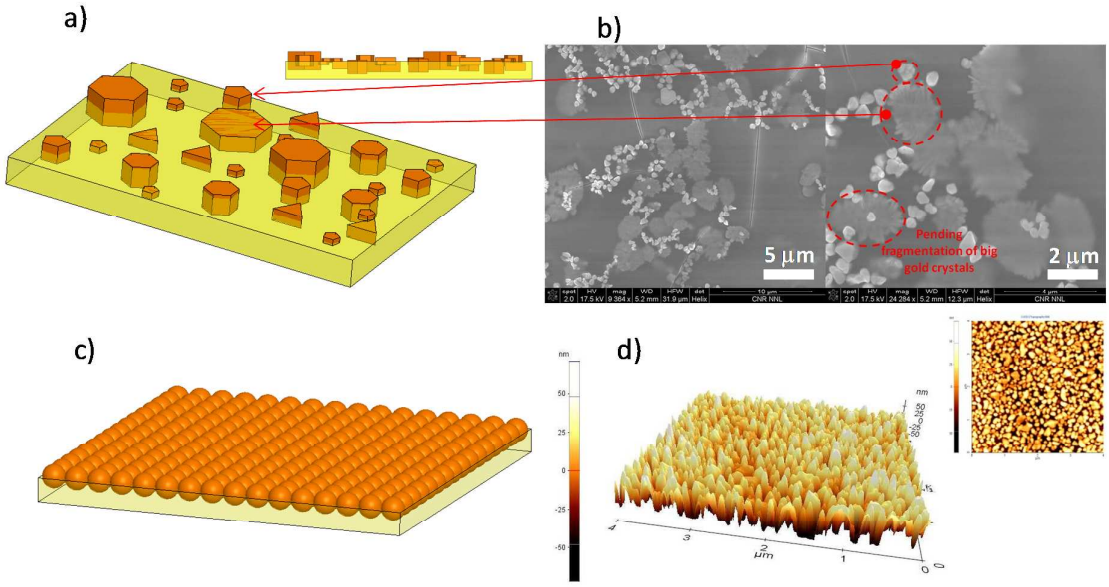

Figure 9: a) Scheme of the fragmentation process. b) Illustrations of the fragmentation mechanism occurring in CTO polymer on gold particles by laser irradiation viewed by SEM images using various scales from small to high magnifications (laser irradiation intensity: 3 J/cm^2, irradiation time: 50s). c) Idealized scheme of the uniform gold patterned layer performed by prolonged irradiation time. d) AFM topography 2D and 3D images of a quasi continuous gold film.

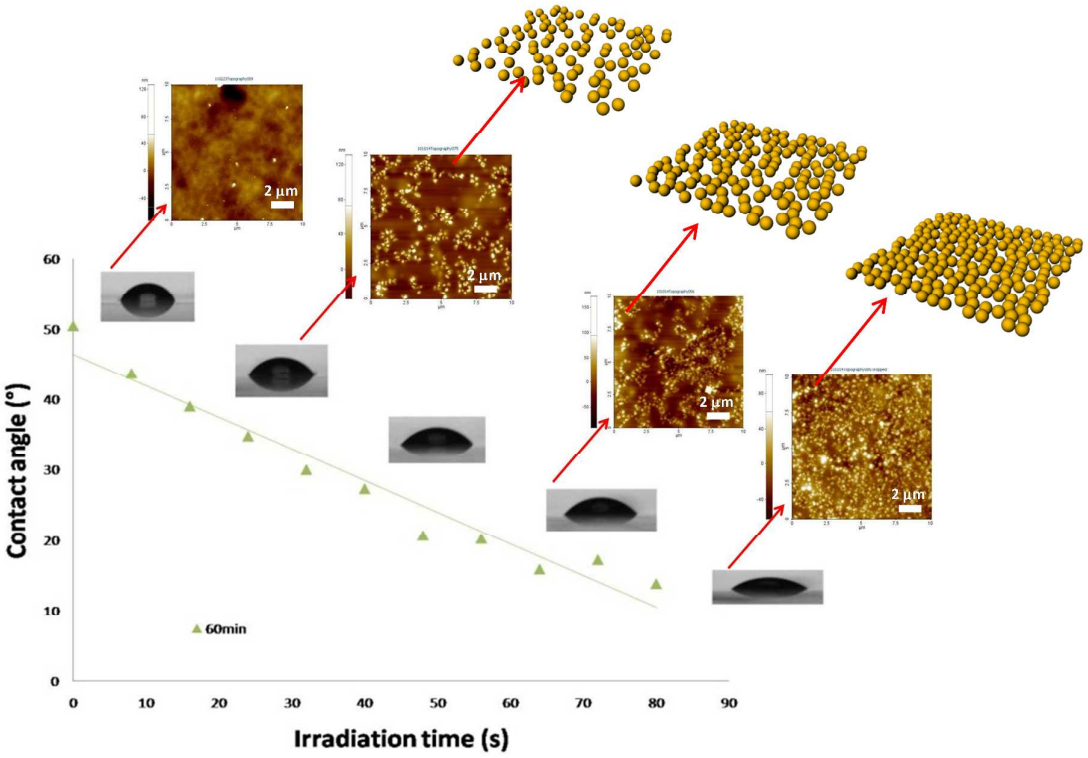

Figure 10: Contact Angle measurements in function of the irradiation time illustrated respectively by their droplet images: Insets: AFM topography images of the gold/CTO surfaces in function of the irradiation times (Fluence 3 J/cm^2) correlated with their GNPs distribution initially schematized in Fig. 1 b).

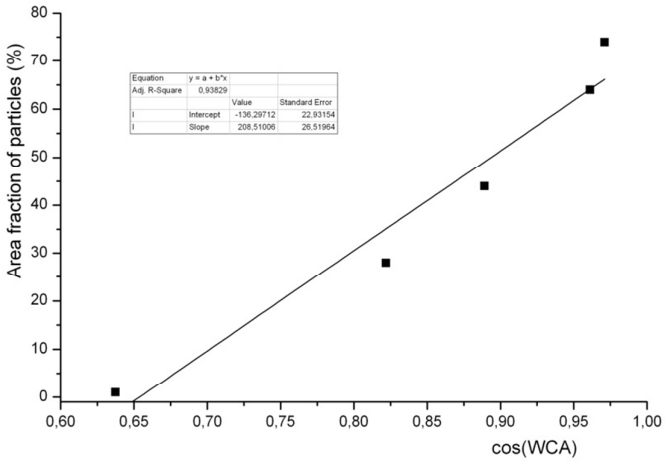

Figure 11: Cosines of the water contact angle versus the area fraction of particles. The area fraction of particles represent the percentage of the area recovered by gold nanoparticles. For each exposure, water contact angles and area fractions of particles are defined allowing to correlate the Cassie equation by the observed linear trend.

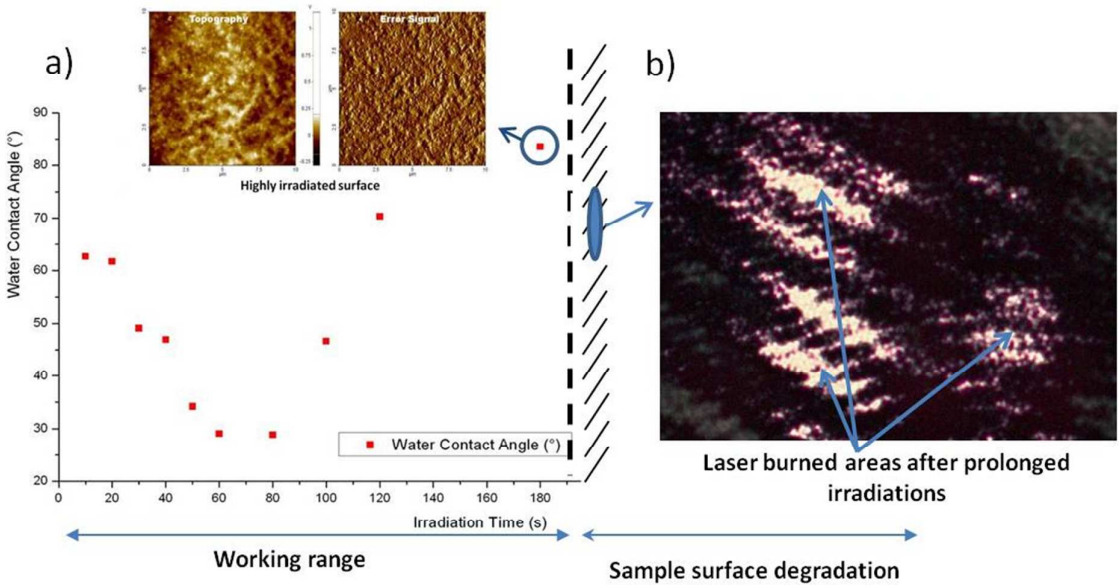

Figure 12: Contact Angle measurements in function of the irradiation time from 10s to 180s. Inset. AFM topography images of the gold/CTO surfaces for highly irradiated surfaces after 180s irradiation time (Fluence 3 J/cm^2). b) Optical image illustrating degraded areas after a prolonged laser irradiation.

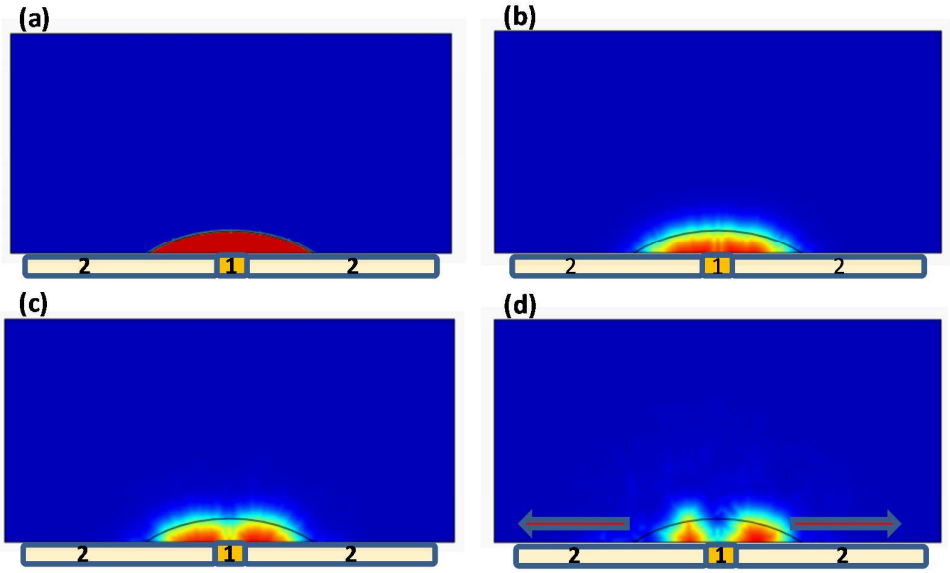

Figure 13: 3D FEM simulation: basic principle of the droplet spreading and separation. The region corresponds to the central region of the device of Fig. 1. Starting from a) to d), time evolution of the droplet spreading at the interface of different contact angle surfaces.

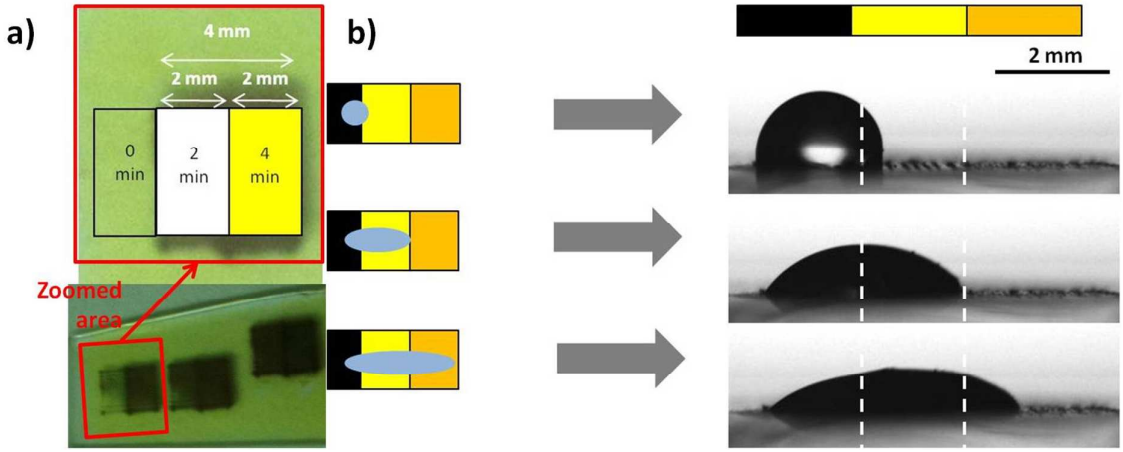

Figure 14: a) Optical microscopy image of the CTO-Au samples after laser irradiation and functionalization; Inset: scheme of the designed area. b) Illustration of the water droplet spreading by optical microscopy images.